AEROSERVOELASTIC BEHAVIOR OF SUPERSONIC GUIDED FLIGHT VEHICLES[*]

M. FATHI [1],[**] A. S. NOBARI[1], M. SABZEHPARVAR[1], M. M. MOGHADDAM[2] AND H. HADDADPOUR[3]

[1]Dept. of Aerospace Engineering, Amirkabir University of Technology, Tehran, I. R. of Iran
Email: phd82129930@aut.ac.ir
[2]Dept. of Mechanical Engineering Group, Tarbiat Modares University, Tehran, I. R. of Iran
[3]Dept. of Aerospace Engineering, Sharif University of Technology, Tehran, I. R. of Iran

Abstract– Flight dynamics of the guided vehicle is modelled by the aid of linear and angular equations of motions using Lagrange's approach in this paper. Governing equations of the control system and the elastic behavior of the vehicle are added to the equations of dynamic states. Flexibility effect is modelled using the normal modes, generalized coordinates and forces. For validation of modified FORTRAN simulation code, the stability of specific vehicles is determined and compared with the same results in the literature. Using this code and by solving the governing equations for the desired flight vehicle, the aeroservoelasticity is analyzed and then the results are compared with the rigid cases and with the flight test data. Errors induced to control system sensors are shown in the figures. Good compatibility is achieved between the simulation and the experimental results. Fast Fourier transformations (FFT) is used for extracting the structural flexibility frequencies from the elastic simulation and flight test data.

Keywords– Aeroservoelasticity, lagrange's approach, generalized coordinates, simulation code, control system

1. INTRODUCTION

Due to the geometric and configuration restrictions, it is usually necessary to install the navigation and control systems far from the center of gravity in guided flight vehicles. The elastic behavior of these vehicles can cause aeroservoelastic instability or deviation from the desired flight path. Control sensors measure erroneous signals and cause the instability problems in operation of the system due to these effects. It is necessary to improve and modify the governing models and to compensate the errors. N-degree of freedom flight simulation must be used to consider the behavior and the trajectory of the flexible flight vehicles. It is also necessary to derive the complex equations of motion containing the elasticity effects.

Linearized equations of motion for spinning missiles were derived by Crimi based on Lagrange's approach [1]. He ignored the structural damping due to over-estimation of computations. For the non-spinning variable-mass rockets (considering the propellant consumption effect), aeroelastic stability was considered by Meirovitch and Wesley [2]. A closed-form approach was developed for determining the static aeroelastic instability of non-spinning rockets flying in the plane without using the full-expanded equations and only by applying the structural effectiveness coefficient by Elyada [3]. Meirovitch and Nelson [4] combined the flight equations with the elastic ones by using Lagrange's method to consider the stability of the spinning elastic flight vehicles. Platus considered this effect for the spinning rockets and

---

proved that in some special cases, the structural damping can cause instability of the spinning missiles [5]. A semi-empirical method was developed by Schmidt for deriving the aeroelastic equations of various flight vehicles in terms of vibration modes [6]. This method was used later for deriving the governing equations of the spinning rockets. Haddadpour derived the equations governing the rigid and elastic motions of an elastic flight vehicle in the presence of the control system by using Lagrange's method to determine aeroservoelastic instability [7]. He used the modal analysis and the generalized coordinates and forces to drive the equations of motion in the time domain and then transferred them to the Laplace domain. He derived an analytic equation by using Routh criterion to analyze the elastic stability of the slender flight vehicles. Pourtakdoost and Asadian derived the nonlinear equations of motion for the elastic missiles [8]. They used the non-uniform beam model under the axial force for deriving the bending vibration equations. Thrust effect in the boost phase of the flight on the vibrational characteristics has also been studied. The effect of structural damping on the chaotic behavior of nonlinear panels in supersonic flow was considered by Pourtakdoost and Fazelzadeh [9]. They considerd the nonlinear governing equations based on Von Karman's large deflection of isotropic flat plates with structural damping. A first order piston theory was utilized for determining the aerodynamic panel loadings. The Galerkin approach was used to transform the nonlinear governing equations into a set of nonlinear ordinary differential equations. The resulting system of equations was solved through a numerical integration scheme. Chaotic analysis was performed using several criteria, results indicate that structural damping highly influences the panel stability boundary and limit cycle amplitude as well as the domain of the chaotic region. Local bifurcation of the attitudinal dynamics of the torque free rigid body motion was discussed by Shirazi and Ghaffari-Saadat [10]. Hamiltonian formalism was used to express equations of motion in this paper. To simplify attitudinal dynamics of a rigid body, six dimensional state space was reduced to a two dimensional one by Andoyer canonical transformation. Non-dimensional parameters of the system were defined and the effects of change in these parameters on the structural stability and the equilibrium points of the reduced space were discussed. The Poincaré surface of the section in the reduced phase space and heteroclinic orbits were derived. Based on the non-dimensional parameters of the system, two and three dimensional bifurcation diagrams were achieved. The study showed that the various types of structural stability could be achieved for torque free rigid body attitudinal dynamics by changing the relative magnitudes of the principal moments of inertia.

The equations of motion for an elastic flight vehicle are derived based on Lagrange's approach and generalized forces and coordinates in the present work. Modal analysis, slender body theory and classical approaches are used for the structural, aerodynamics and control system analysis, respectively. The prepared flight simulation code is executed for the cases presented in the literature after linearization of the equations. Finally, the simulation code is executed for the desired specific flight vehicle to determine the flexibility effect on the control system and the flight path and then the results are compared with the flight test data.

2. LAGRANGE'S EQUATIONS

General form of the Lagrange's equation for the generalized coordinates and forces is as follows:

$$\frac{d}{dt}\left(\frac{\partial T}{\partial \dot{q}_i}\right) - \frac{\partial T}{\partial q_i} + \frac{\partial U}{\partial q_i} + \frac{\partial D}{\partial \dot{q}_i} = Q_i \tag{1}$$

where T is the kinetic energy, U is the potential energy, D is the Rayleigh dissipation damping function and q_i is ith generalized coordinate. Lagrange's equations in body-fixed coordinates are as follows [1]:

$$\begin{cases} \dfrac{\mathrm{d}}{\mathrm{dt}}\left(\dfrac{\partial \mathrm{T}}{\partial \mathrm{p}}\right) - \mathrm{r}\dfrac{\partial \mathrm{T}}{\partial \mathrm{q}} + \mathrm{q}\dfrac{\partial \mathrm{T}}{\partial \mathrm{r}} = \mathrm{M_x} \\[2mm] \dfrac{\mathrm{d}}{\mathrm{dt}}\left(\dfrac{\partial \mathrm{T}}{\partial \mathrm{q}}\right) - \mathrm{p}\dfrac{\partial \mathrm{T}}{\partial \mathrm{r}} + \mathrm{r}\dfrac{\partial \mathrm{T}}{\partial \mathrm{p}} = \mathrm{M_y} \\[2mm] \dfrac{\mathrm{d}}{\mathrm{dt}}\left(\dfrac{\partial \mathrm{T}}{\partial \mathrm{r}}\right) - \mathrm{q}\dfrac{\partial \mathrm{T}}{\partial \mathrm{p}} + \mathrm{p}\dfrac{\partial \mathrm{T}}{\partial \mathrm{q}} = \mathrm{M_z} \end{cases} \tag{2}$$

$$\begin{cases} \dfrac{\mathrm{d}}{\mathrm{dt}}\left(\dfrac{\partial \mathrm{T}}{\partial \mathrm{u}}\right) - \mathrm{r}\dfrac{\partial \mathrm{T}}{\partial \mathrm{v}} + \mathrm{q}\dfrac{\partial \mathrm{T}}{\partial \mathrm{w}} = \mathrm{F_x} \\[2mm] \dfrac{\mathrm{d}}{\mathrm{dt}}\left(\dfrac{\partial \mathrm{T}}{\partial \mathrm{v}}\right) - \mathrm{p}\dfrac{\partial \mathrm{T}}{\partial \mathrm{w}} + \mathrm{r}\dfrac{\partial \mathrm{T}}{\partial \mathrm{u}} = \mathrm{F_y} \\[2mm] \dfrac{\mathrm{d}}{\mathrm{dt}}\left(\dfrac{\partial \mathrm{T}}{\partial \mathrm{w}}\right) - \mathrm{q}\dfrac{\partial \mathrm{T}}{\partial \mathrm{u}} + \mathrm{p}\dfrac{\partial \mathrm{T}}{\partial \mathrm{v}} = \mathrm{F_z} \end{cases} \tag{3}$$

In the above equations, (u,v,w) are linear velocity, (p,q,r) are angular velocity, (M_x, M_y, M_z) are moment and (F_x, F_y, F_z) are force components in the body coordinate axis. Displacement of each element of the vehicle in terms of the normal vibration modes are as follows [11]:

$$\begin{cases} \theta = \sum_{i=1}^{n} \theta_i(x)\gamma_i(t) \\[2mm] \delta_y = \sum_{i=1}^{n} \varphi_i(x)\,\eta_i(t) \\[2mm] \delta_z = \sum_{i=1}^{n} \varphi_i(x)\,\zeta_i(t) \end{cases} \tag{4}$$

where $\varphi_i(x)$ is the ith normal bending mode shape and $\eta_i(t)$ and $\zeta_i(t)$ are the corresponding generalized coordinates. Also, $\theta_i(x)$ is the ith torsional vibration mode and $\gamma_i(t)$ is the corresponding generalized coordinates. By considering the vehicle as a beam and using bending and torsional vibration differential equations [12], the displacement of each element of the vehicle in accordance with Fig. 1 will be as follows:

$$\begin{cases} e_x = 0 \\[2mm] e_y = \delta_y - z\theta_x = \sum_{i=1}^{n}\left(\varphi_i\eta_i - z\theta_i\gamma_i\right) \\[2mm] e_z = \delta_z + y\theta_x = \sum_{i=1}^{n}\left(\varphi_i\zeta_i + y\theta_i\gamma_i\right) \end{cases} \tag{5}$$

where $\delta_x, \delta_y, \delta_z$ are the position vector components of the displaced point after bending and e_x, e_y, e_z are the position vector components of the displaced point after torsion.
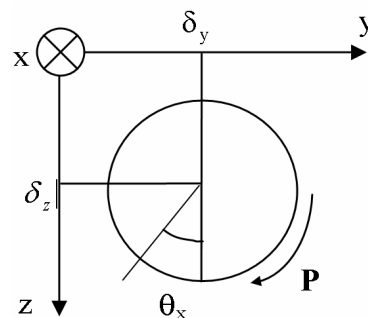

Fig. 1. Section of elastic vehicle in body fixed coordinates

3. KINETIC AND POTENTIAL ENERGIES AND DAMPING FUNCTION

In Fig. 2, relations between the position vectors of each point are as follows:

$$\begin{cases} \vec{E} = \vec{R} + \vec{r} \\ \vec{r} = \vec{r}_0 + \vec{e} \end{cases} \tag{6}$$

where $\vec{E}$ and $\vec{R}$ are the position vectors of the vehicle center of gravity and each point of the deformed body in the inertial coordinates respectively. $\vec{r}_0$ and $\vec{r}$ are the position vectors of each point of the vehicle before and after deformation in the body coordinates respectively. Kinetic energy due to the rigid and elastic motions is as follows:

$$T = \frac{1}{2}\int_m \frac{dE}{dt}\bigg|_I \cdot \frac{dE}{dt}\bigg|_I dm = \frac{1}{2}m\vec{V}_I.\vec{V}_I + \frac{1}{2}I\left(r^2+q^2\right) + \frac{1}{2}I_x p^2 + \frac{1}{2}\left(p^2 + \frac{q^2+r^2}{2}\right)\sum_{i=1}^{n}J_i\gamma_i^2 + \frac{1}{2}\sum_{i=1}^{n}J_i\dot{\gamma} +$$

$$\frac{1}{2}\sum_{i=1}^{n}M_i\left[\dot{\eta}_i^2 + \dot{\zeta}_i^2 + p^2\left(\zeta_i^2 + \eta_i^2\right) + \left(q\zeta_i - r\eta_i\right)^2 - 2p\left(\dot{\eta}_i\zeta - \dot{\zeta}_i\eta_i\right)\right] \tag{7}$$

where I_x and I are the vehicle moments of inertia about the longitudinal and the lateral axis respectively. M_i and J_i are the generalized masses correspondent to the ith bending and torsional modes. Potential energy is computed as follows:

$$U = \frac{1}{2}\int_L EI\left[\left(\frac{\partial^2\delta_y}{\partial x^2}\right)^2 + \left(\frac{\partial^2\delta_z}{\partial x^2}\right)^2\right]dx + \frac{1}{2}\int_L GJ\left(\frac{\partial\theta}{\partial x}\right)^2 dx = \frac{1}{2}\sum_{i=1}^{n}M_i\omega_i^2\left(\eta_i^2 + \zeta_i^2\right) + \frac{1}{2}\sum_{i=1}^{n}J_i\psi_i^2\gamma_i^2 \tag{8}$$

where EI is the bending and GJ is the torsional stiffness of the vehicle respectively. Rayleigh dissipation function will be achieved in terms of the generalized force and coordinates [12]:

$$D = \frac{1}{2}\sum_{i=1}^{n}2\mu_i\omega_i M_i\left(\dot{\eta}_i^2 + \dot{\zeta}_i^2\right) + \frac{1}{2}\sum_{i=1}^{n}2\upsilon_i\psi_i J_i\dot{\gamma}_i^2 \tag{9}$$

where μ_i and υ_i are the ith bending and torsional modal dampings respectively. Generalized forces in the right-hand side of the Lagrange's equations are as follows:

$$\begin{cases} Q_{\eta_i} = \int_L f_y(x,t)\varphi_i(x)dx \\ Q_{\zeta_i} = \int_L f_z(x,t)\varphi_i(x)dx \\ Q_{\gamma_i} = \int_L m_x(x,t)\theta_i(x)dx \end{cases} \tag{10}$$

where $m_x(x,t)$ is the distributed longitudinal moment, $f_y(x,t)$ and $f_z(x,t)$ are the distributed side and lift aerodynamic forces respectively. After determination of the kinetic energy, potential energy, Rayleigh dissipation function and generalized forces, extraction of the equations will be presented in the next section.

4. ELASTIC DEFORMATIONS

Using the virtual works, kinetic and potential energies and putting them in the Lagrange's equations and defining η_i , ζ_i and γ_i as the generalized coordinates, we will have:

$$\ddot{\eta}_i + 2\mu_i\omega_i\dot{\eta}_i - 2p\dot{\zeta}_i + \left(\omega_i^2 - p^2 - r^2\right)\eta_i + (qr - \dot{p})\zeta_i = \frac{1}{M_i}\int_L f_y(x,t)\varphi_i(x)\,dx \tag{11}$$

$$\ddot{\zeta}_i + 2\mu_i\omega_i\dot{\zeta}_i + 2p\dot{\eta}_i + \left(\omega_i^2 - p^2 - q^2\right)\zeta_i + (qr + \dot{p})\eta_i = \frac{1}{M_i}\int_L f_z(x,t)\varphi_i(x)\,dx \tag{12}$$

$$\ddot{\gamma}_i + 2\upsilon_i\dot{\gamma}_i\psi_i + \left(\psi_i^2 - p^2 - \frac{q^2 + r^2}{2}\right)\gamma_i = \frac{1}{J_i}\int_L m(x,t)\theta_i(x)\,dx \tag{13}$$
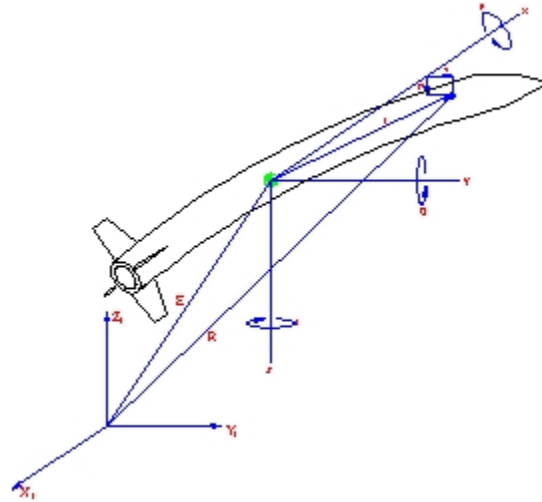

Fig. 2. Inertial and body fixed coordinates

5. ANGULAR VELOCITY EQUATIONS

Lagrange's equations for the moments shown in relation 2 are written in the body fixed coordinate system. Putting the kinetic energy equation into those relations and assuming $I_y = I_z = I$ results in:

$$\left(I_x + \sum_{i=1}^n J_i\gamma_i^2 + \sum_{i=1}^n M_i\left(\eta_i^2 + \zeta_i^2\right)\right)\dot{p} + 2\left(\sum_{i=1}^n J_i\gamma_i\dot{\gamma}_i + \sum_{i=1}^n M_i\left(\zeta_i\dot{\zeta}_i + \eta_i\dot{\eta}_i\right)\right)p$$
$$-\sum_{i=1}^n M_i\left[\left(\ddot{\eta}_i\zeta_i - \ddot{\zeta}_i\eta_i\right) + (q\eta_i - r\zeta_i)(q\zeta_i - r\eta_i)\right] = M_x \tag{14}$$

$$\left(I - I_m + \sum_{i=1}^n M_i\zeta_i^2 + \frac{1}{2}\sum_{i=1}^n J_i\gamma_i^2\right)\dot{q} + pr\left(I_x - I + \sum_{i=1}^n M_i\zeta_i^2 + \frac{1}{2}\sum_{i=1}^n J_i\gamma_i^2\right)$$
$$+ (pq - \dot{r})\sum_{i=1}^n M_i\zeta_i\eta_i + 2q\sum_{i=1}^n M_i\zeta_i\dot{\zeta}_i - 2r\sum_{i=1}^n M_i\zeta_i\dot{\eta}_i + q\sum_{i=1}^n J_i\gamma_i\dot{\gamma}_i = M_y \tag{15}$$

$$\left(I - I_m + \sum_{i=1}^n M_i\eta_i^2 + \sum_{i=1}^n J_i\gamma_i^2\right) + pq\left(I - I_x - \sum_{i=1}^n M_i\eta_i^2 - \frac{1}{2}\sum_{i=1}^n J_i\gamma_i^2\right)$$
$$-(pr + \dot{q})\sum_{i=1}^n M_i\eta_i\zeta_i + 2r\sum_{i=1}^n M_i\eta_i\dot{\eta}_i - 2q\sum_{i=1}^n M_i\dot{\zeta}_i\eta_i + r\sum_{i=1}^n J_i\gamma_i\dot{\gamma}_i = M_z \tag{16}$$

where $I_m = mx_{cg}^2$ is due to the displacement of instantaneous center of gravity relative to the origin of the body fixed coordinate.

6. ANGLE OF ATTACK EQUATIONS

Similarly for the angles of attack, putting the kinetic energy equation into the relation 3 results in:

$$\begin{cases} m(\dot{u} + qw - rv) = F_{exb} \\ m(\dot{v} + ru - pw) = F_{eyb} \\ m(\dot{w} + pv - qu) = F_{ezb} \end{cases} \tag{17}$$

The forces in the right-hand side of these equations are derived in the body fixed coordinate system.

7. EXTERNAL MOMENTS

Moments in the right-hand side of the equations 14 to 16 are the summation of the external moments due to the aerodynamic lift, control and thrust forces. Moment equations are derived as follows:

$$M_x = -\sum_{k=1}^{m}\sum_{i=1}^{n}\int_{A_{w_k}}\left[L_{\alpha w_k}\left(r_{w_k}\right)+L_{\beta w_k}\left(r_{w_k}\right)\right]r_{w_k}\left[p+\dot{\gamma}_i(t)\theta_i(x_{w_k})\right]dA_{w_k}+M_x^c \tag{18}$$

$$M_y = -\int xL_\alpha(x)\alpha(x,t)dx+\sum_{i=1}^{n}x_{w_k}L_\alpha\left(x_{w_k}\right)\alpha\left(x_{w_k},t\right)+F_{Tx}\sum_{i=1}^{n}\zeta_i(t)\varphi_i(x_T)-F_{Tx}x_T\sum_{i=1}^{n}\zeta_i(t)\varphi_i'(x_T)$$
$$+F_{Ax}\sum_{i=1}^{n}\zeta_i(t)\varphi_i(x_D)+M_y^c \tag{19}$$

$$M_z = -\int xL_\beta(x)\beta(x,t)dx-\sum_{k=1}^{m}x_{w_k}L_\beta\left(x_{w_k}\right)\beta\left(x_{w_k},t\right)-F_{Tx}\sum_{i=1}^{n}\eta_i(t)\varphi_i(x_i)$$
$$-F_{Tx}x_T\sum_{i=1}^{n}\eta_i(t)\varphi_i'(x_T)-F_{Ax}\sum_{i=1}^{n}\eta_i(t)\varphi_i(x_D)+M_z^c \tag{20}$$

where x_{w_k} is the distance of kth row of wings, x_D and x_T are the distance of drag and thrust resultant forces acting points from the center of mass respectively. r_k is the area element distance from the root on each wing of the kth row. M_x^c, M_y^c and M_z^c are the control moments.

8. EXTERNAL FORCES

Forces in the right-hand side of 17 are the summation of the aerodynamic lift, control and thrust forces. Force equations are derived as follows:

$$F_{exb} = F_{Tx}+F_{Ax}+F_x^c \tag{21}$$

$$F_{eyb} = -\int L_\beta(x)\beta(x,t)dx-\sum_{k=1}^{m}L_{\beta w_k}\beta\left(x_{w_k},t\right)+F_{Tx}\sum_{i=1}^{n}\eta_i(t)\varphi_i'(x_T)+F_{Ax}\sum_{i=1}^{n}\eta_i(t)\varphi_i'(x_D)+F_y^c \tag{22}$$

$$F_{ezb} = -\int L_\alpha(x)\alpha(x,t)dx-\sum_{k=1}^{m}L_{\alpha w_k}\alpha\left(x_{w_k},t\right)+F_{Tx}\sum_{i=1}^{n}\zeta_i(t)\varphi_i'(x_T)+F_{Ax}\sum_{i=1}^{n}\zeta_i(t)\varphi_i'(x_D)+F_z^c \tag{23}$$

9. AEROELASTIC DEFLECTIONS

Considering equations 10 and using the Eqs. (21) to (23), the elastic deflections are derived as follows:

$$\int m(x,t)\theta_i(x)dx = -\sum_{k=1}^{m}\sum_{i=1}^{n}\theta_i\left(x_{w_k}\right)\int_{A_{w_k}}\left[L_{\alpha v_k}\left(r_{w_k}\right)+L_{\beta w_k}\left(r_{w_k}\right)\right]r_{w_k}\left[p+\dot{\gamma}_i(t)\theta_i(x)\right]dA_{w_k} \tag{24}$$

$$\int f_y(x,t)\varphi_i(x)dx = -\int_L L_\beta(x)\beta(x,t)\varphi_i(x)dx-\sum_{k=1}^{m}\sum_{i=1}^{n}L_\beta\left(x_{w_k},t\right)\varphi_i\left(x_{w_k}\right)$$
$$F_{Tx}\sum_{i=1}^{n}\eta_i(t)\varphi_i'(x_T)\varphi_i(x_T)+F_{Ax}\sum_{i=1}^{n}\eta_i(t)\varphi_i'(x_D)\varphi_i(x_D) \tag{25}$$

$$\int f_z(x,t)\varphi_i(x)dx = -\int_L L_\alpha(x)\alpha(x,t)\varphi_i(x)dx-\sum_{k}\sum_{i}L_\alpha\left(x_{w_k},t\right)\varphi_i\left(x_{w_k}\right)+$$
$$F_{Tx}\sum_{i}\zeta_i(t)\varphi_i'(x_T)\varphi_i(x_T)+F_{Ax}\sum_{i}\zeta_i(t)\varphi_i'(x_D)\varphi_i(x_D) \tag{26}$$

10. SUMMARY OF EQUATIONS

Expansion of $\alpha(x,t)$, $\beta(x,t)$ over the length of the vehicle and also expansion of $\alpha\left(x_{w_k},t\right)$, $\beta\left(x_{w_k},t\right)$ at the installing position of the wings are as follows:

$$\begin{cases} \alpha(x,t) = \alpha_0 - \sum_{i=1}^{n} \zeta_i(t)\varphi_i'(x) + \frac{1}{u}\sum_{i=1}^{n} \dot{\zeta}_i(t)\varphi_i(x) - \frac{q}{u}x \\[2mm] \beta(x,t) = \beta_0 - \sum_{i=1}^{n} \eta_i(t)\varphi_i'(x) + \frac{1}{u}\sum_{i=1}^{n} \dot{\eta}_i(t)\varphi_i(x) - \frac{r}{u}x \\[2mm] \alpha(x_{w_k},t) = \alpha_{0w_k} - \sum_{i=1}^{n} \zeta_i(t)\varphi_i'(x_{w_k}) + \frac{1}{u}\sum_{i=1}^{n} \dot{\zeta}_i(t)\varphi_i(x_{w_k}) - \frac{q}{u}x_{w_k} \\[2mm] \beta(x_{w_k},t) = \beta_{0w_k} - \sum_{i=1}^{n} \eta_i(t)\varphi_i'(x_{w_k}) + \frac{1}{u}\sum_{i=1}^{n} \dot{\eta}_i(t)\varphi_i(x_{w_k}) - \frac{r}{u}x_{w_k} \end{cases} \tag{27}$$

Assuming $L_\alpha(x) = L_\beta(x)$, the following parameters are defined:

$$\begin{cases} \int_L L_\alpha(x)\varphi_i(x)dx = \int_L L_\beta(x)\varphi_i(x)dx = I_1^i \\[2mm] \int_L xL_\alpha(x)\varphi_i(x)dx = \int_L xL_\beta(x)\varphi_i(x)dx = I_2^i \\[2mm] \int_L L_\alpha(x)\varphi_i'(x)dx = \int_L L_\beta(x)\varphi_i'(x)dx = I_3^i \\[2mm] \int_L xL_\alpha(x)\varphi_i'(x)dx = \int_L xL_\beta(x)\varphi_i'(x)dx = I_4^i \\[2mm] \int_L L_\alpha(x)\varphi_i^2(x)dx = \int_L L_\beta(x)\varphi_i^2(x)dx = I_5^i \\[2mm] \int_L L_\alpha(x)\varphi_i(x)\varphi_i'(x)dx = \int_L L_\beta(x)\varphi_i(x)\varphi_i'(x)dx = I_6^i \end{cases} \tag{28}$$

In order to track the path of the vehicle, the translational equations of the motion of the vehicle must be transferred from body fixed coordinate system to the inertial coordinate system by using a transfer function. Transferring of $\vec{F}_B$ to $\vec{F}_I$ is as follows:

$$\vec{F}_I = C_B^I \vec{F}_B \tag{29}$$

Using the Euler parameters, one can write for C_B^I as follows:

$$C_B^I = \begin{bmatrix} a^2 + b^2 + c^2 - d^2 & 2(bc - ad) & 2(ac + bd) \\ 2(ad + bc) & a^2 - b^2 + c^2 - d^2 & 2(cd - ab) \\ 2(db - ac) & 2(ab + cd) & a^2 - b^2 - c^2 + d^2 \end{bmatrix} \tag{30}$$

where a,b,c and d are the Euler parameters (quaternions).
By using the above definitions for driving the forces in the inertial coordinates we will have:

$$F_{exb} = F_{Ax} + F_{Tx} + F_x^c \tag{31}$$

$$F_{eyb} = \sum_{i=1}^{n} \eta_i(t)I_3^i - \frac{1}{u}\sum_{i=1}^{n} \dot{\eta}_i(t)I_1^i + \sum_{k=1}^{m}\sum_{i=1}^{n} \eta_i(t)L_{\beta w_k}(x_{w_k})\varphi_i'(x_{w_k}) - \frac{1}{u}\sum_{k=1}^{m}\sum_{i=1}^{n} \dot{\eta}_i(t)L_{\beta w_k}(x_{w_k})\varphi_i(x_{w_k}) + \sum_{i=1}^{n} \eta_i(t)\varphi_i'(x_T)F_{Tx}$$

$$+ \sum_{i=1}^{n} \eta_i(t)\varphi_i'(x_D)F_{Ax} + F_{Ay} + F_{Ty} - rJ_{T1} + F_y^c \tag{32}$$

$$F_{ezb} = \sum_{i=1}^{n} \zeta_i(t)I_3^i - \frac{1}{u}\sum_{i=1}^{n} \dot{\zeta}_i(t)I_1^i + \sum_{k=1}^{m}\sum_{i=1}^{n} \zeta_i(t)L_{\alpha w_k}(x_{w_k})\varphi_i'(x_{w_k}) - \frac{1}{u}\sum_{k=1}^{m}\sum_{i=1}^{n} \dot{\zeta}_i(t)L_{\alpha w_k}(x_{w_k})\varphi_i(x_{w_k}) + \sum_{i=1}^{n} \zeta_i(t)\varphi_i'(x_T)F_{Tx}$$

$$+ \sum_{i=1}^{n} \zeta_i(t)\varphi_i'(x_D)F_{Ax} + F_{Az} + F_{Tz} + qJ_{T1} + F_z^c \tag{33}$$

$$\begin{bmatrix} F_{xI} \\ F_{yI} \\ F_{zI} \end{bmatrix} = C_B^I \begin{bmatrix} F_{exb} \\ F_{eyb} \\ F_{ezb} \end{bmatrix} + \begin{bmatrix} F_{Gx} \\ F_{Gy} \\ F_{Gz} \end{bmatrix} \tag{34}$$

Finally, the governing state differential equations will be as follows:

$$
\begin{cases}
\dot{X}(t) = V_X \\
\dot{Y}(t) = V_Y \\
\dot{Z}(t) = V_Z
\end{cases}
\tag{35}
$$

$$
\begin{cases}
\dot{V}_x(t) = \dfrac{F_{xI}}{m} \\[2mm]
\dot{V}_y(t) = \dfrac{F_{yI}}{m} \\[2mm]
\dot{V}_z(t) = \dfrac{F_{zI}}{m}
\end{cases}
\tag{36}
$$

$$
\begin{cases}
\dot{p}(t) = \left[M_{Ax} + M_{Tx} + \sum_{k=1}^{m}\sum_{i=1}^{n} L_{P_{w_k}} \dot{\gamma}_i(t)\theta_i(x_{w_k}) \right] \Big/ I_x \\[3mm]
\dot{q}(t) = \left[M_{Ay} + (I - I_x - I_m)pr + M_{Ty} - qF_{J2} + x_{cg}F_{ezb} - I_4^i\sum_{i=1}^{n}\zeta_i(t) + \dfrac{1}{u}I_2^i\sum_{i=1}^{n}\dot{\zeta}_i(t) - \right. \\[3mm]
\sum_{k=1}^{m}\sum_{i=1}^{n} x_{w_k} L_{\alpha w_k}(x_{w_k})\varphi_i'(x_{w_k})\zeta_i(t) + \dfrac{1}{u}\sum_{k=1}^{m}\sum_{i=1}^{n} x_{w_k} L_{\alpha w_k}(x_{w_k})\varphi_i(x_{w_k})\dot{\zeta}_i(t) + \sum_{i=1}^{n}\zeta_i(t)\varphi_i(x_T)F_{Tx} - \\[3mm]
\left. \sum_{i=}^{n}\zeta_i(t)\varphi_i'(x_T)x_T F_{Tx} + \sum_{i=1}^{n}\zeta_i(t)\varphi_i(x_D)F_{Ax} \right] \Big/ (I - I_m) \\[3mm]
\dot{r}(t) = \left[M_{Az} + (I_x - I + I_m)pq + M_{Tz} - rF_{J2} + x_{cg}F_{eyb} + I_4^i\sum_{i=1}^{n}\eta_i(t) - \dfrac{1}{u}I_2^i\sum_{i=1}^{n}\dot{\eta}_i(t) + \right. \\[3mm]
\sum_{k=1}^{m}\sum_{i=1}^{n} x_{w_k} L_{\beta w_k}(x_{w_k})\varphi_i'(x_{w_k})\eta_i(t) - \dfrac{1}{u}\sum_{k=1}^{m}\sum_{i=1}^{n} x_{w_k} L_{\beta w_k}(x_{w_k})\varphi_i(x_{w_k})\dot{\eta}_i(t) - \sum_{i=1}^{n}\eta_i(t)\varphi_i(x_T)F_{Tx} + \\[3mm]
\left. \sum_{i=1}^{n}\eta_i(t)\varphi_i'(x_T)x_T F_{T(x)} - \sum_{i=1}^{n}\eta_i(t)\varphi_i(x_D)F_{Ax} \right] \Big/ (I - I_m)
\end{cases}
\tag{37}
$$

$$
\begin{cases}
\ddot{\zeta}_i(t) = \dfrac{1}{M_i}\left[-\alpha_0 I_1^i + \sum_{i=1}^{n}\zeta_i(t)I_6^i - \dfrac{1}{u}\sum_{i=1}^{n}\dot{\zeta}_i(t)I_5^i + \dfrac{q}{u}I_2^i - \sum_{k=1}^{m}\sum_{i=1}^{n} L_{\alpha w_k}(x_{w_k})\alpha_{0w_k}\varphi_i(x_{w_k}) + \right. \\[3mm]
\sum_{k=1}^{m}\sum_{i=1}^{n} L_{\alpha w_k}(x_{w_k})\varphi_i(x)\varphi_i'(x)\zeta_i(t) - \dfrac{1}{u}\sum_{k=1}^{m}\sum_{i=1}^{n} L_{\alpha w_k}(x_{w_k})\varphi_i^2(x_{w_k})\dot{\zeta}_i(t) + \dfrac{q}{u}\sum_{k=1}^{m}\sum_{i=1}^{n} x_{w_k} L_{\alpha w_k}(x_{w_k})\varphi_i(x_{w_k}) \\[3mm]
\left. + \sum_{i=1}^{n}\zeta_i(t)\varphi_i(x_T)\varphi'(x_T)F_{Tx} + \sum_{i=1}^{n}\zeta_i(t)\varphi_i(x_D)\varphi'(x_D)F_{Ax} \right] - 2\mu_i\omega_i\dot{\zeta}_i(t) - 2p\dot{\eta}(t) - (\omega_i^2 - p^2)\zeta_i(t) \\[3mm]
\ddot{\eta}_i(t) = \dfrac{1}{M_i}\left[-\beta_0 I_1^i + \sum_{i=1}^{n}\eta_i(t)I_6^i - \dfrac{1}{u}\sum_{i=1}^{n}\dot{\eta}_i(t)I_5^i + \dfrac{r}{u}I_2^i - \sum_{k=1}^{m}\sum_{i=1}^{n} L_{\beta w_k}(x_{w_k})\beta_{0w_k}\varphi_i(x_{w_k}) + \right. \\[3mm]
\sum_{k=1}^{m}\sum_{i=1}^{n} L_{\beta w_k}(x_{w_k})\varphi_i(x)\varphi_i'(x)\eta_i(t) - \dfrac{1}{u}\sum_{k=1}^{m}\sum_{i=1}^{n} L_{\beta w_k}(x_{w_k})\varphi_i^2(x_{w_k})\dot{\eta}_i(t) + \dfrac{r}{u}\sum_{k=1}^{m}\sum_{i=1}^{n} x_{w_k} L_{\beta w_k}(x_{w_k})\varphi_i(x_{w_k}) \\[3mm]
\left. + \sum_{i=1}^{n}\eta_i(t)\varphi_i(x_T)\varphi_i'(x_T)F_{Tx} + \sum_{i=1}^{n}\eta_i(t)\varphi_i(x_D)\varphi_i'(x_D)F_{Ax} \right] - 2\mu_i\omega_i\dot{\eta}_i(t) - 2p\dot{\zeta}_i(t) - (\omega_i^2 - p^2)\eta_i(t) \\[3mm]
\ddot{\gamma}_i(t) = \dfrac{1}{J_i}\left[M_{Ax} + \sum_{k=1}^{m}\sum_{i=1}^{n} L_{pw_k}\theta_i^2(x_{w_k})\dot{\gamma}(t) \right] - 2\upsilon_i\psi_i\dot{\gamma}(t) - (\psi_i^2 - p^2)\gamma_i(t)
\end{cases}
\tag{38}
$$

$$\begin{cases} \dot{a}(t) = -\frac{1}{2}\big[b(t)p(t) + c(t)q(t) + d(t)r(t)\big] \\[2mm] \dot{b}(t) = -\frac{1}{2}\big[a(t)p(t) + c(t)r(t) - d(t)q(t)\big] \\[2mm] \dot{c}(t) = \frac{1}{2}\big[a(t)q(t) - b(t)r(t) + d(t)p(t)\big] \\[2mm] \dot{d}(t) = \frac{1}{2}\big[a(t)r(t) + b(t)q(t) - c(t)p(t)\big] \end{cases} \tag{39}$$

The above mentioned equations define the elastic vehicle motions and by solving them with a fourth order Runge-Kutta method, forces, moments, elastic deformations, angular and linear velocities of the vehicle will be determined in the time domain.

11. CONTROL SYSTEM MODELING

For determinig the interactions of structural flexibility, aerodynamics, control system and flight dynamics, it is necessary to add the model of the control system to the aeroelastic one. In this specific vehicle, there are three control channels. Channels one and two are from the tracking type. Channel three is from the regulatory type. Channels 1 and 2 have two control loops.

The internal loop is for stabilizing the vehicle about the lateral axes. The outer one is for keeping it on the desired trajectory. In this vehicle, the lateral acceleration commands are the control variables named C1 and C2 respectively. Figure 3 indicates the vehicle body fixed coordinates and the positive directions of the commands. C1 and C2 commands are executed by channels I and II. Channel III is responsible for preventing the vehicle from rolling.
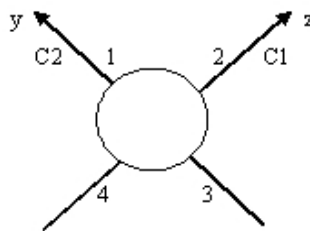
Fig. 3. Fin numbering, axis and command directions in body
fixed coordinates (Aft view of vehicle)

12. CHANNELS I AND II (PITCH AND YAW)

Control loops for these channels are shown in Fig. 4. In each internal stabilizing loop, there is one rate gyro for measuring the vehicle angular velocities about y or z body fixed axes. Each outer loop has a linear accelerometer which measures the vehicle acceleration in the y or z directions. The transfer functions of the accelerometers and the rate gyros are given in Tables 1 and 2.
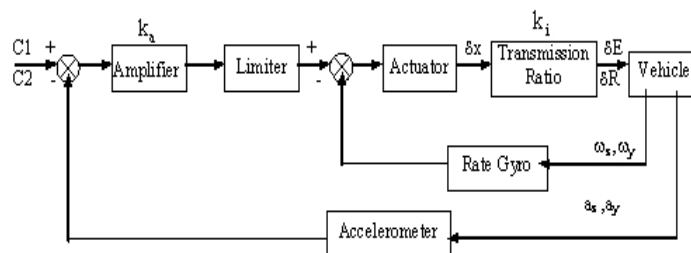
Fig. 4. Closed-Loop control system for channels I and II

M. Fathi et al.

Table 1. Transfer functions of accelerometers

Item	Accelerometers
Transfer function	$g_a\left(\dfrac{\omega_a^2}{s^2 + 2\omega_a \xi_a s + \omega_a^2}\right)$

Table 2. Transfer functions of rate gyros

Item	Rate gyros
Transfer function	$g_r\left(\dfrac{\omega_r^2}{s^2 + 2\omega_r \varsigma_r s + \omega_r^2}\right)$

Control loop for channel III is shown in Fig. 5. This channel is simpler than the channels I and II, because it's only function is to stabilize the roll of the vehicle. The transfer function of the free gyro is presented in Table 3 and for the actuator in Table 4.
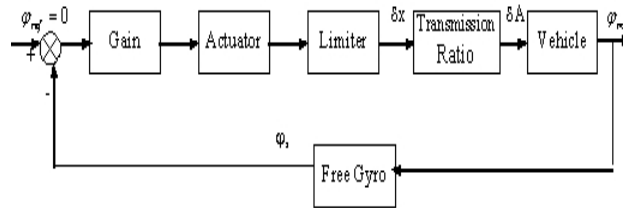
Fig. 5. Closed-Loop control system for channel III

Table 3. Transfer function of free gyro

Item	Free gyro
Transfer function	$g_f\left(\dfrac{1}{1 + t_f s}\right)$

Table 4. Transfer function of actuator

Item	Actuator
Transfer function	$g_{act}\left(\dfrac{s + z_{act}}{(s + p_1)(s + p_2)}\right)$

13. VALIDATION OF THE CODE

It was necessary to verify the generated code by simulating the flight dynamics of the two cases given in Ref. 5. The required parameters of these vehicles were derived from the data presented in the reference. Dynamic pressures equivalent to the static aeroelastic instabilities are determined by executing the modified flight simulation code and the results are tabulated in Table 5 in comparison with the results of Ref. 5. The results of this simulation are also shown in Figs. 6 and 7.
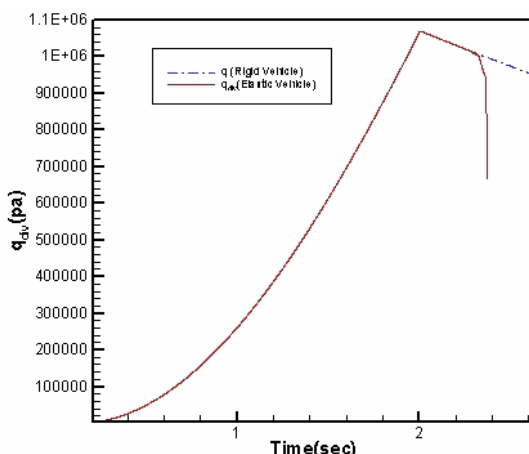
Fig. 6. Divergence dynamic pressure for vehicle A
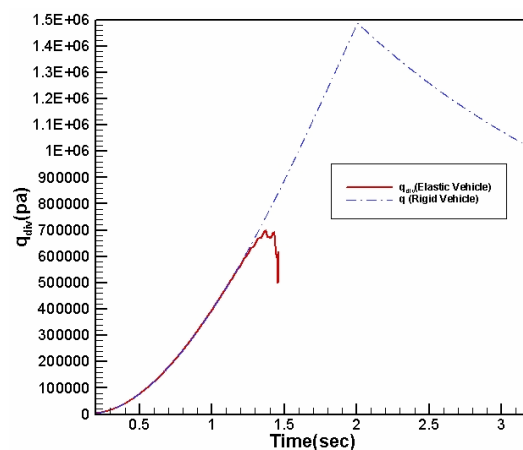
Fig. 7. Divergence dynamic pressure for vehicle B

14. RESULTS

Structural flexibility of the vehicle at the sensor positions causes measuring extra angular velocities and lateral accelerations. For considering these effects, it seemed necessary to analyze the time variations of

the angular velocities and lateral accelerations resulting from the modified flight simulation. Validation of the modified code before applying to the desired flight vehicle was necessary. Modified flight simulation code was executed for the cases presented in Ref. 5 and good compatibility was achieved which proved the validity of the prepared code. First bending and torsional mode shapes and their related frequencies were determined using fem code as input to the simulation program. Also, slope curve of bending mode shape was inputed to the program using the prepared fem code. For executing the FEM code, it was necessary to determine the distributed properties of the desired vehicle. These distributed properties are shown in Figs. 8a and 8b. The curves derived from the code are shown in the Figs. 9a to 9c. Initial values of the time dependant elastic deflection functions are presented in Table 6. The first bending and torsional mode frequencies and damping coefficient are presented in Table 7. The simulation results for elastic and rigid vehicles are plotted and compared with the flight test data. Time histories of the angular velocities for these three states and for one channel are shown in Fig. 10a. These three curves are quite compatible but the fluctuations due to structural flexibility are obvious in the elastic simulation and flight test data. Part of these curves are shown in Fig. 10b for better judgment. Time histories of the lateral accelerations for the 2nd channel are presented in Fig. 11a. The above mentioned explanations are valid for these accelerations too. Part of these curves are also shown in Fig. 11-b for better comparison. Fluctuation frequency of simulated roll rate matches the resulted torsional modal analysis frequency. Time histories of the roll angle and roll rate are presented in Fig. 12. Simulation program was executed for the elastic and rigid cases to present the flexibility effects on the desired flight path deviation. The results are shown in Fig. 13. Fast Fourier Transformations (FFT) on the data of the 2nd channel's rate gyro and accelerometer are shown in Figs. 14a and 14b for extracting the structural flexibility frequencies from elastic simulation and flight test data.

Table 5. Comparison table for dynamic pressures
equivalent to aeroelastic instabilities

Vehicle	$q_{div}(N/m^2)$	Reference
Test Case A	1.149e6	Elyada
Test Case B	6.576e5	Elyada
Test Case A	1.013e6	Present Work
Test Case B	6.700e5	Present Work

Table 6. Initial value of parameters
for time functions

Parameter	Initial value
η_0	0.2
$\dot{\eta}_0$	1.0
ζ_0	0.2
$\dot{\zeta}_0$	1.0
γ_0	0.0005
$\dot{\gamma}_0$	0.0

Table 7. First bending and torsional mode shape frequencies
and their damping coefficients

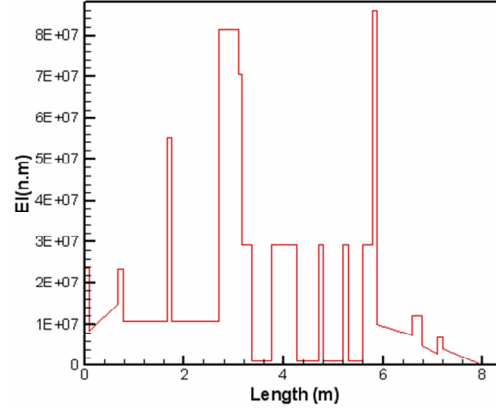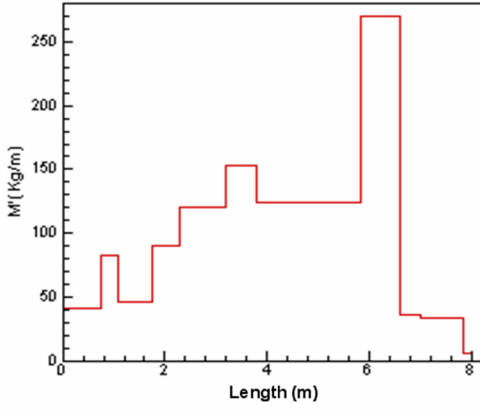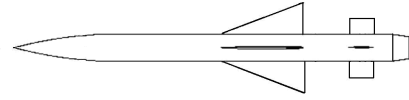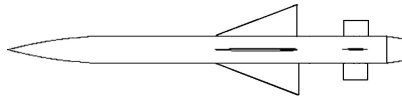| Item	υ	μ	ω(rad/s)	ψ(rad/s)
Value	0.05	0.05	90	1639
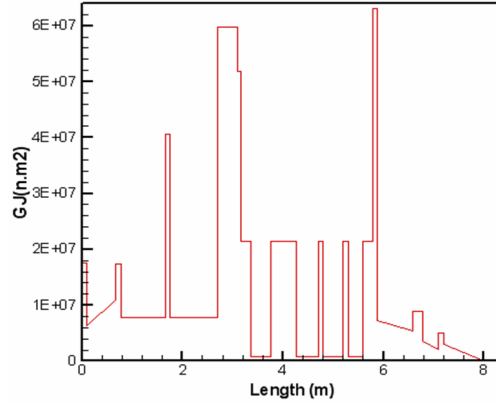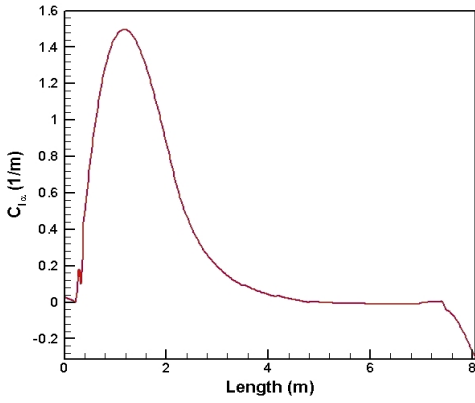
Fig. 8a. Desired vehicle distributed properties   Fig. 8b. Desired vehicle distributed properties(continue)
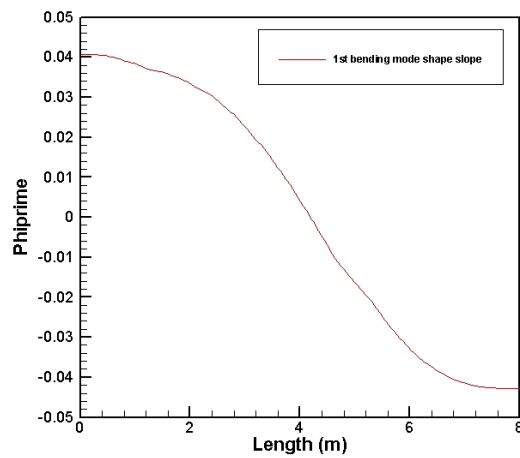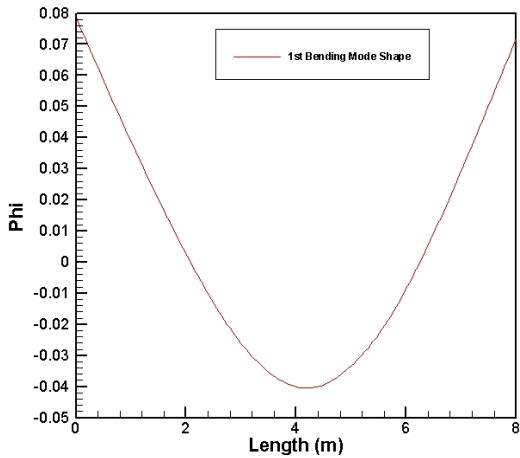

Fig. 9a. Bending elastic mode shape   Fig. 9b. Slope of bending elastic mode shape
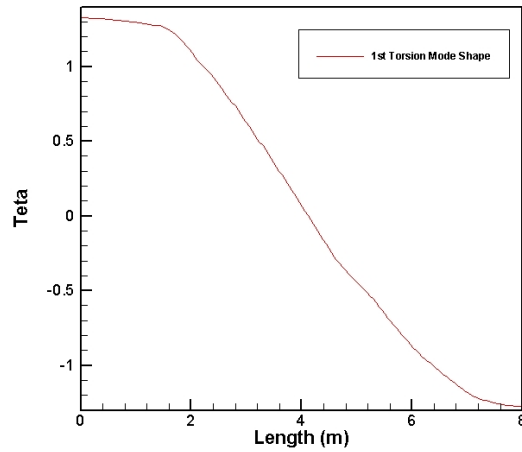
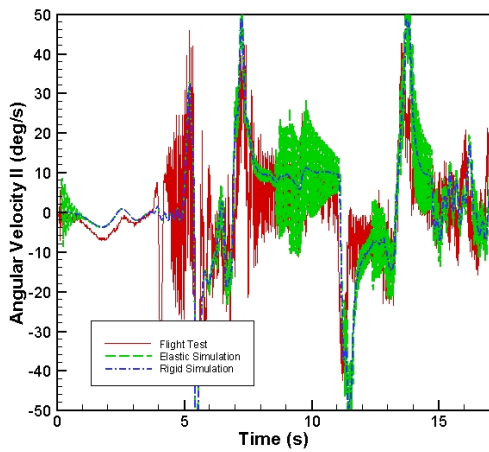Fig. 9c. Torsional elastic mode shape

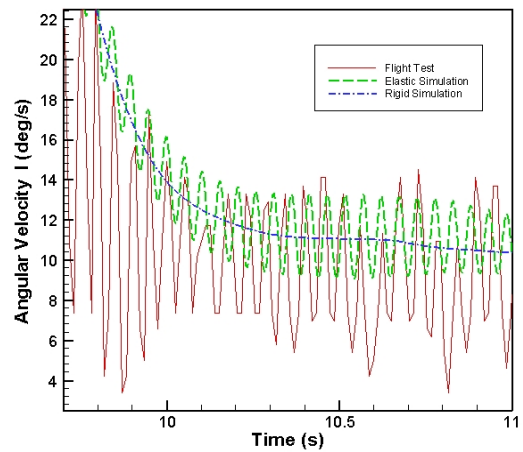Fig. 10a. Angular velocity of channel II
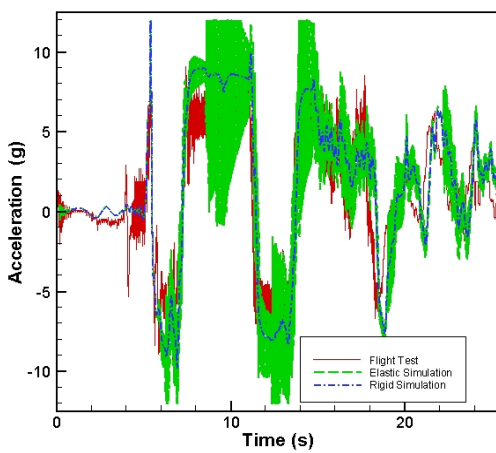

Fig. 10b. Zoom in angular velocity curve

Fig. 11a. Lateral acceleration of Channel II

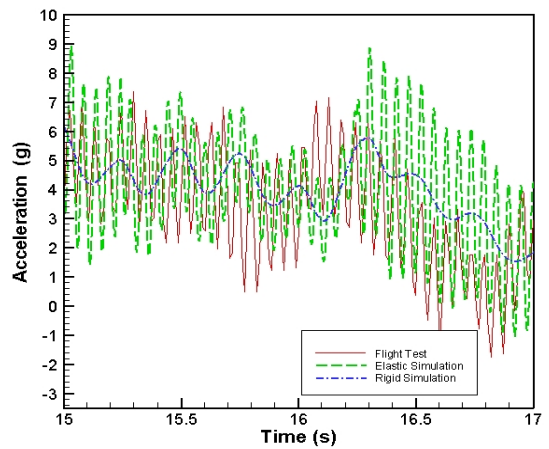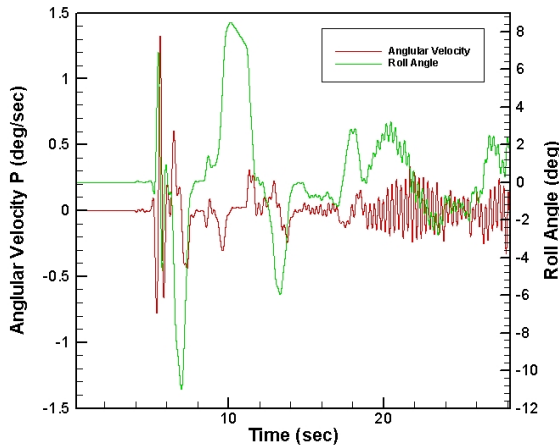Fig. 11b. Zoom in lateral acceleration curve
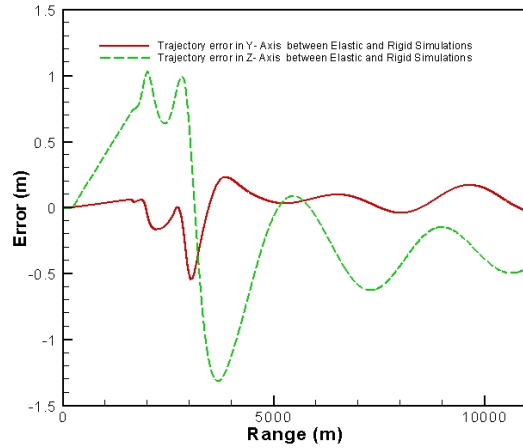
Fig. 12. Roll rate and roll angle

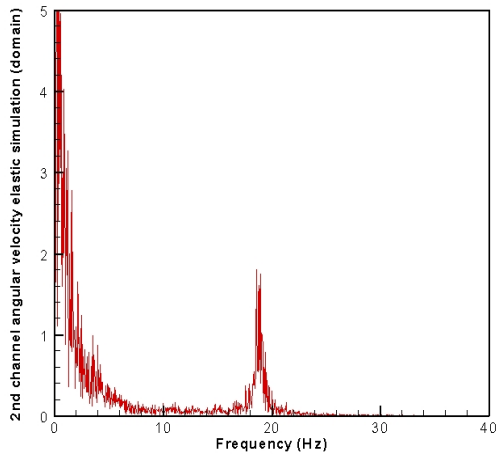Fig. 13. Flexibility effect on flight-vehicle desired trajectory

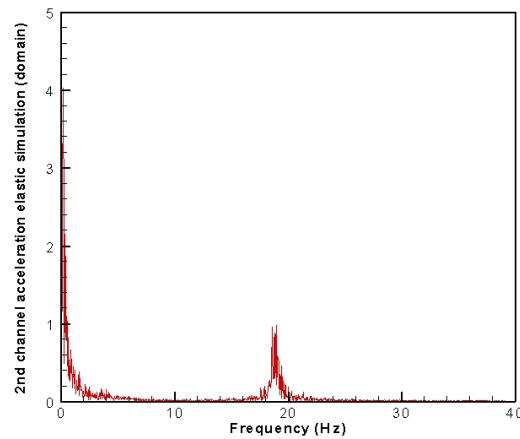Fig. 14a. FFT on 2nd channel Angular velocity elastic simulation and flight test data

Fig. 14b. FFT on 2nd channel Acceleration elastic simulation and flight test data

15. CONCLUSION

Elastic equations of motion for a flexible flight vehicle were added to the equations of rigid body motion and control system states. Validation of the generated flight simulation code were approved by solving these equations and applying them to the special cases presented in Ref. 5 and comparing with the flight test data. In the next step the code was executed for the specific vehicle under consideration and the results were presented in the tables and figures. As seen from the angular velocity and the lateral acceleration curves, there is acceptable coincidence between simulation and modal analysis oscillation frequencies. It is shown that the structural flexibility can cause a considerable deviation from the desired flight path in two planes. These deviations were derived and shown for their importance.

REFERENCES

1. Crimi, P. (1984). Aeroelastic stability and response of flexible tactical weapons. AIAA Paper 84-0392.

2. Meirovitch, L. & Wesley, D. A. (1967). On the dynamic characteristics of a variable mass slender elastic body under high accelerations. *AIAA Journal*, Vol. 5, No. 8, pp. 1439-1447

3. Elyada, D. (1989). Closed-form approach to rocket vehicles aeroelastic divergence. *Journal of Spacecraft and Rockets*, Vol. 26. No.2.

4. Meirovitch, L. & Nelson, H. D. (1966). On the high-spin motion of a satellite containing elastic parts.

Journal of Spacecraft and Rockets, Vol. 3, pp. 1597- 1602.

5. Platus, D. H. (1992). Aeroelastic stability of slender, spinning vehicles. *Journal of Guidance*, Vol. 15, No. 1.

6. Bilimoria, K. D. & Schmidt, D. K. (1995). Integrated development of the equations of motion for elastic hypersonic flight vehicles. *Journal of Guidance,* Vol. 18, No. 1.

7. Haddadpour, H. (2006). Aeroservoelastic stability of supersonic slender-body flight vehicles. *Journal of Guidance, Control, and Dynamics*, Vol. 29. No. 6.

8. Pourtakdoust, S. H. & Assadian, N. (2002). Aeroelastic Analysis of guided hypersonic launch vehicles. Accepted for the publication in the Journal of Science and Technology.

9. Pourtakdoust, S. H. & Fazelzadeh, S. A. (2003). Effect of structural damping on chaotic behavior of nonlinear panel flutter. *Iranian Journal of Science and Technology, Transaction B, Engineering*, Vol. 27, No, B3, pp. 453-467.

10. Shirazi, K. H. & Ghaffari-Saadat, M. H. (2003). Local bifurcation in torque free rigid body motion. *Iranian Journal of   Science and Technology, Transaction B, Engineering*, Vol. 27, No. B3, pp. 493-506.

11. Bisplinghoff, R. L. & Ashley, H. (1986). *Principles of aeroelasticity*. John Wiley and Sons, Inc., New York, 1962.

12. Meirovitch, L. (1986). Elements of vibration analysis. McGraw-Hill.